Control of Mutual Coupling in High-Field MRI Transmit Arrays in the Presence of High-Permittivity Liners

published in

IEEE Transactions on Microwave Theory and Techniques

DOI: 10.1109/TMTT.2017.2668406

Atefeh Kordzadeh, Student member, IEEE, Nicola De Zanche, Senior Member, IEEE

***Abstract*— In high-field MRI, transmit arrays and high-permittivity inserts are often used together to mitigate the effects of RF field inhomogeneities due to short wavelength. However, array performance is limited by mutual impedance between elements which must be closely spaced around the volume of interest. Mutual impedance plays a substantial role at high frequencies and is increased by the presence of dielectric pads which are used to increase the homogeneity of the RF magnetic field. This paper describes a decoupling strategy for an eight-channel transmit/receive array in the presence of a high permittivity dielectric liner. The elements are decoupled using capacitive bridges between adjacent elements. In spite of the higher mutual impedance due to the liner, both mutual resistance and reactance can be removed between adjacent elements (isolation better than 30 dB), and coupling between non-adjacent elements is maintained below 15 dB. The effects of decoupling on the transmit performance of the array in presence of high permittivity liners are investigated in terms of coupling, magnetic field intensity, SAR and transmit efficiencies.**

***Index Terms*— Magnetic resonance imaging, transmit array coils, specific absorption rate, mutual impedance, decoupling, high permittivity liner.**

I. Introduction

MAGNETIC resonance imaging (MRI) at high static fields provides higher SNR, and consequently faster imaging and higher resolution than MRI at standard field strengths ($B_0 \leq 3$ tesla) [1]. However, higher magnetic fields result in higher Larmor frequencies ($f_0 = \gamma B_0$, $\gamma = 42.576\ MHz/T$ for ^{1}H) and thus shorter radio frequency wavelengths. The wavelength in human tissues is also shorter than that in vacuum because of the permittivity and is thus comparable to or shorter than the body's dimensions. The short wavelength leads to undesirable inhomogeneous RF magnetic fields (circularly polarized transverse component, $\mathbf{B}_1^+$), and consequently inhomogeneous image excitation, as well as increased coupling between array elements.

High dielectric constant (HDC) pads placed between the sample and the array have been used to improve RF field homogeneity within the region of interest (ROI) [2]. Pads with relative permittivity higher than 100 have been extensively used to focus magnetic field locally and hence increase SNR in an ROI [3]. They are made by mixing powdered ceramics such as barium or calcium titanate ($BaTiO_3$ and $CaTiO_3$) with deuterium oxide (D_2O) or deionized water, forming a suspension that is then sealed in plastic bags. The resulting permittivity depends on the volume ratio and the dielectric constants of each of the materials [4], [5].

Array excitation with adjustment of amplitude and phase of each element (i.e., RF shimming) mitigates the RF inhomogeneities inside the ROI and also provides control over specific absorption rate (SAR) [6]. Besides requiring a multichannel system, mutual coupling is the most important challenge to implementing transmit arrays. The proximity of the elements in an array gives rise to significant mutual impedance between them through which signal and noise can transfer. Additionally, when loaded with lossy materials such as the human body, elements in an array will share common eddy current loops inside the sample [7], resulting in mutual resistance and consequently noise correlation [6], [8]. Mutual impedance increases when HDC pads are used [9] and thus one of the goals of this work is to explore whether the enhanced interaction can be suppressed with practical methods.

Coupling is more difficult to manage at higher frequencies and strongly affects the field maps of individual elements. Parallel transmit techniques (e.g., transmit SENSE [10]) require a distinct field map for each element. Therefore it is reasonable to require high isolation (>30 dB) between adjacent elements to avoid significant overlap in the sensitivity patterns. Coupling also affects the transmit efficiency of the array [11], because power coupled between ports returns down the transmit path and is dissipated to protect the power amplifiers. The minimum isolation required between all pairs of elements to achieve a given efficiency depends on the specific excitation method and settings (e.g., RF shimming settings, transmit SENSE pulse shapes) [11]. Nevertheless, because the array elements are tuned resonators, in practice it is desirable to achieve a minimum of 15–20 dB isolation to avoid detuning effects.

Different techniques have been used to decouple the elements in a coil array [6], [8], [12], [13], [14], [15], [16] where most of them aim to remove mutual reactance as the most significant term in the mutual impedance. The simplest method to remove mutual inductance is to overlap adjacent loops in an array [8].

This work was supported in part by the Natural Sciences and Engineering Research Council (Canada).

A. Kordzadeh is in the joint PhD program in the Departments of Biomedical Engineering, and Electrical and Computer Engineering at University of Alberta, Edmonton, Canada. T6G 2R3 (email: kordzade@ualberta.ca).

N. De Zanche is a medical physicist with Alberta Health Services and an associate professor in the Department of Oncology of the University of Alberta, Edmonton, Canada. T6G 1Z2 (email: dezanche@ieee.org)

Scholarships from the University of Alberta are gratefully acknowledged.

Although this method effectively reduces coupling levels between adjacent elements, it is not optimal for parallel spatial encoding where the elements' sensitivity patterns should have minimal overlap and be distinct from each other [17]. Therefore in receive-only arrays, low-input impedance (reflective) preamplifiers are used to further reduce inductive coupling between non adjacent elements by blocking currents on the array elements [8]. However, this technique is not practical in transmit mode due to the lack of powerful high-output-impedance amplifiers [18]. More recently magnetic walls, implemented using metamaterials, have been used to isolate adjacent elements by suppressing the common fields between elements. This technique yields approximately 26 dB isolation between neighboring channels at 7T [19], [20]. Numerous methods employing capacitors and inductors between elements have also been devised to remove mutual inductance [13], [14], [15], [16], [21]. Capacitive networks are more popular decoupling circuits due to higher quality factors than inductive circuits, resulting in higher SNR [14].

Until recently, the resistive term of the mutual impedance

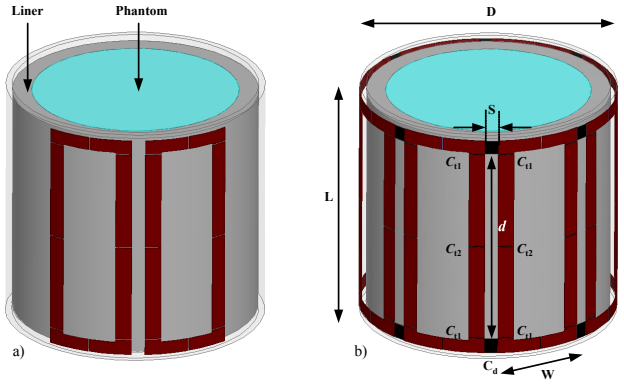

Figure 1: a) Two loops conformed to a cylindrical phantom in presence of a high-permittivity dielectric liner. b) Designed eight channel array. (D=200 mm, L=180 mm, W=69 mm, S=10 mm).

was simply ignored or believed to be impossible to remove [22]. Recently-developed methods to eliminate the mutual resistance in receive arrays are investigated in [6] and [13]. It is expected that eliminating mutual resistance in transmit arrays will be beneficial where high-output-impedance power amplifier decoupling cannot be used.

This work describes an eight-channel transmit/receive array of loops for 4.7 tesla. A high permittivity liner is located between the coil array and phantom to improve the magnetic field homogeneity inside the ROI [23]. As a result, mutual coupling is also significantly enhanced between elements. Hence both resistive and reactive components of the mutual impedance between elements are eliminated using capacitive bridges appropriately placed between adjacent loops. Transmit performance metrics such as $\mathbf{B}_1^+$ field pattern and SAR are used to investigate the effect of decoupling. For comparison, real and imaginary components of the mutual impedance are removed individually as well as concomitantly, and results are compared to the coupled case in terms of transmit and safety efficiencies [23].

In [24] we investigated the effect of removing both mutual reactance and resistance between three elements in a concave array which is used to scan the occipital lobe of the brain. As a result we were able to reduce coupling to –44 dB between adjacent channels ensuring a distinct field pattern for each element. We expand on our abstract by extending the array to 8 channels to image the whole head, providing the corresponding simulations and experimental data. The larger number of channels greatly increases the number of interactions between elements and complicates practical construction. We also expand the theoretical analysis of coupling in section II-A and show how and why coupling changes with the dielectric liner. Additional simulation and fabrication details are also provided in sections II-B, C and D. Simulation results as well as bench measurements and imaging results are outlined in section III.

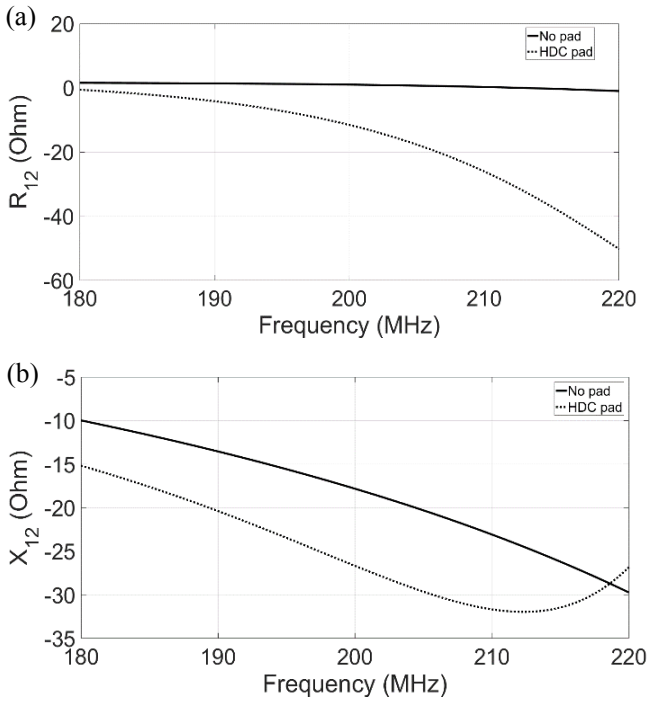

Figure 2: Simulated (a) mutual resistance, (b) mutual reactance (with HDC liner: solid, without: dotted) for the two-loop example of Figure 1a. Note that in the absence of both liner and phantom X_{12} would be inductive.

II. Methods

A. Theory

Mutual impedance between coupled elements, Z_{12}, is a complex quantity with a real part, R_{12}, and imaginary part, X_{12}, through which signal and noise transfer. To explain the effect of dielectric liners on the mutual impedance, we must examine Ampere's law with Maxwell's correction in a conductive medium (1),

$$\nabla \times \boldsymbol{H} = \boldsymbol{J}_D + \boldsymbol{J}_C = j\omega\varepsilon\boldsymbol{E} + \sigma\boldsymbol{E}\,, \qquad (1)$$

where $\boldsymbol{H}$ is the magnetic field (A/m), $\boldsymbol{E}$ is the electric field (V/m), ω is the angular frequency, $\boldsymbol{J}_D$ is the displacement current density and $\boldsymbol{J}_C$ is conduction current density (A/m^2). Displacement current density depends on the frequency as well as permittivity. Using an HDC liner with high permittivity (>150) will create a significant displacement current density which acts as a secondary source to generate additional

magnetic fields [3]. The higher the permittivity of the liner, the stronger the electric/magnetic field generated in the region adjacent to it.

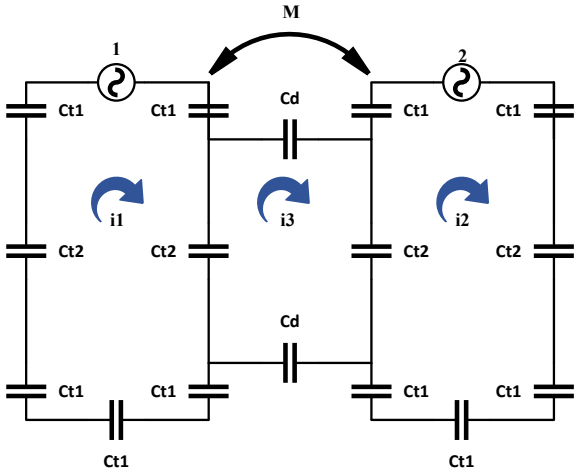

Figure 3: Circuit model for coupled loops with decoupling capacitors.

Mutual impedance can be calculated using reaction theory [25] from the electromagnetic fields produced by exciting each element. The interaction of two fields i and j, $\langle i,j \rangle$, excited by current sources is defined as [25]

$$< i,j >= \int \boldsymbol{E}^i \cdot \boldsymbol{I}^j dl = I^j \int \boldsymbol{E}^i \cdot d\boldsymbol{l} = -V^i I^j \,, \tag{2}$$

where $\boldsymbol{E}^j$ is the electric field induced by current $\boldsymbol{I}^j$ on coil j, and V^i is the voltage at the ports of coil i. The mutual impedance between elements i and j is then: [25], [26]

$$Z_{ij} = -\frac{<j,i>}{I_i I_j}, \tag{3}$$

$$Z_{ij} = \frac{-1}{I_i I_j}\left\{\iiint_{phantom} \boldsymbol{E}^j(r)\cdot \boldsymbol{J}_p^i(r)dv + \iiint_{pad} \boldsymbol{E}^j(r)\cdot \boldsymbol{J}_p^i(r)dv + \iiint_{coil} \boldsymbol{E}^j(r)\cdot \boldsymbol{J}_c^i(r)dv\right\}. \tag{4}$$

The term $\boldsymbol{J}_c^i(r)$ is the current density on coil i and $\boldsymbol{J}_p^i(r)$ is the current density generated in the phantom and HDC liner (considered to be a single region). In fact $\boldsymbol{J}_p^i$ is the current density in the phantom which is induced by the fields generated by coil i [26]. The displacement current term due to the presence of the HDC liner cannot be ignored and the mutual impedance can be expanded to

$$Z_{ij} = \frac{-1}{I_i I_j}\left\{\iiint_p \sigma_p \boldsymbol{E}^j(r)\cdot \boldsymbol{E}^i(r)dv + \iiint_p j\omega\varepsilon \boldsymbol{E}^j(r)\cdot \boldsymbol{E}^i(r)dv + \iiint_c \boldsymbol{E}^j(r)\cdot \boldsymbol{J}_c^i(r)dv\right\}. \tag{5}$$

Here ε is the permittivity of the phantom or liner, and σ_p is the phantom's conductivity.

Consider two rectangular loops conformed to a cylindrical phantom and corresponding high permittivity liner as shown in Figure 1a. Using full-wave simulation software (HFSS V.15, Ansys Corp., Canonsburg, PA), mutual impedance between two adjacent loops on the cylinder is plotted for the case without and in presence of the dielectric liner in Figure 2. As can be seen at 200 MHz both terms of the mutual impedance have significantly increased with the HDC liner present which is consistent with the above equations for mutual impedance (specifically the third term of (5)).

TABLE I
CAPACITOR VALUES AND LOCATIONS FOR EACH CASE.

	C_{t1} (pF)	C_{t2} (pF)	C_d (pF)	d (mm)
Coupled	15	15	-	-
R_{12}**=0**	14	10	470	25
X_{12}**=0**	10	10	460	30
Z_{12}**=0**	18	10	12	80

To remove mutual impedance between adjacent elements, capacitive bridges are connected between the elements, thus introducing a third current loop [13]. The circuit model of two loops with capacitive decoupling is shown in Figure 3. The current in the third loop is controlled with capacitors C_{t2} and C_d, and their spacing, d. Circuit mesh equations are as follows:

$$\begin{bmatrix} j\omega L + \frac{5}{j\omega C_{t1}} + \frac{2}{j\omega C_{t2}} + R_1 & \frac{-1}{j\omega C_{t2}} & \\ \frac{-1}{j\omega C_{t2}} & \frac{2}{j\omega C_d} + \frac{2}{j\omega C_{t2}} + R_3 & \dots \\ j\omega M + R_{12} & \frac{-1}{j\omega C_{t2}} & \\ & j\omega M + R_{12} & \\ \dots & \frac{-1}{j\omega C_{t2}} & \\ & j\omega L + \frac{5}{j\omega C_{t1}} + \frac{2}{j\omega C_{t2}} + R_1 & \end{bmatrix} \times \begin{bmatrix} i1 \\ i3 \\ i2 \end{bmatrix} = \begin{bmatrix} v1 \\ 0 \\ v2 \end{bmatrix} \tag{9}$$

Here M is the mutual inductance and R_1 and R_3 refer to the self-resistances of the main loops and decoupling loop, respectively. The mutual resistance and reactance between the two ports simplify to:

$$\text{Real}\,(Z_{12}) = \tag{10}$$
$$= R_{12} + \frac{R_3\omega^2 C_{t2}^2}{R_3^2\omega^4 C_{t2}^4 + 4\omega^2(C_{t2} + {C_{t2}^2}/{C_d})^2}$$

$$\text{Imaginary}\,(Z_{12}) = \tag{11}$$
$$= \omega M + \frac{2\omega(C_{t2} + {C_{t2}^2}/{C_d})}{R_3^2\omega^4 C_{t2}^4 + 4\omega^2(C_{t2}^2 + {C_{t2}^2}/{C_d})^2}$$

The mutual impedance is removed by finding appropriate values for C_{t2} and C_d, as well as the separation, d, which directly influences R_3. A few parameter sweeps are performed in HFSS around an initial estimate to determine the desired values. Four cases are compared: no decoupling (coupled), zero mutual resistance (R_{12}=0), zero mutual reactance (X_{12}=0) and zero mutual impedance (Z_{12}=0). Design parameters are listed in Table I.

B. Design and simulation

The coil array designed as shown in Figure 1b consists of eight rectangular loops conformed to an acrylic (PMMA) cylinder supporting copper traces. The former's 200 mm diameter can accommodate a child's head or the extremities.

Capacitors are designed to make the elements resonate at 200.4 MHz which is the Larmor frequency for ^{1}H at 4.7 T. These capacitors are distributed along the coil to guarantee a uniform current distribution on the coil. A lossy cylindrical phantom (160 mm ⌀) with relative dielectric constant $\varepsilon_r = 76$ and conductivity of $\sigma = 0.8\,S/m$ is used to mimic the dielectric properties of brain. An HDC liner with permittivity $\varepsilon_r = 150$ surrounds the phantom to maximize the homogeneity of the magnetic field in the phantom.

Simulation of the array structure is done in HFSS using 50 Ω lumped port excitations (1 W incident power) to acquire scattering parameters. Excitation phase is incremented linearly spanning [0, 2π] to generate a circularly polarized (quadrature) mode. Single-element fields are obtained by exciting the ports with 1 A current sources.

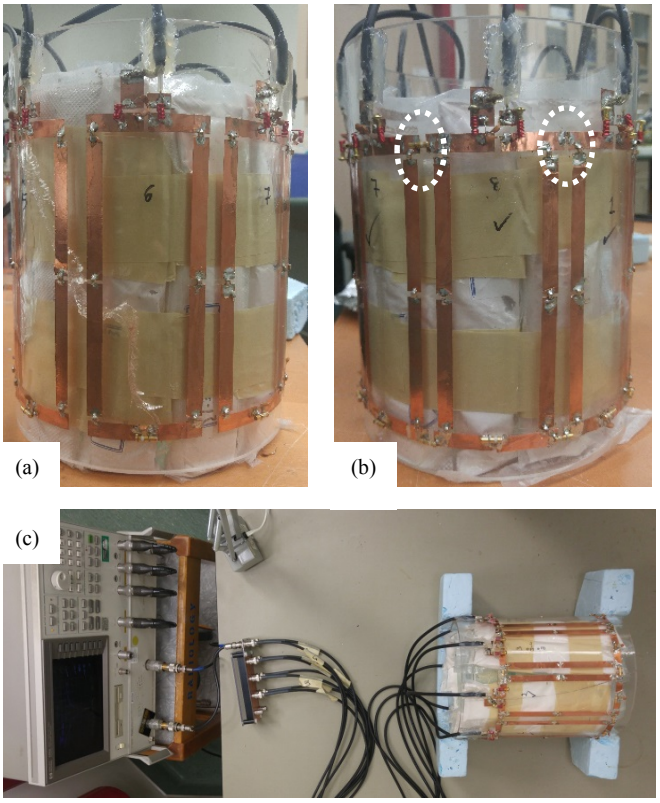

Figure 4: Fabricated arrays (a) coupled, and (b) decoupled using capacitive bridges (dashed ellipses). Bench measurement setup is shown in c), including VNA and the common grounding plate for the 8 coaxes.

C. Fabrication

The array is constructed using adhesive copper tape attached to the PMMA cylinder (Figure 4 (a)). Each element is fine-tuned to 200.4 MHz using a 12 pF trimmer, and matched to 50 Ω using a lattice matching balun. The solution in the phantom (3.6 g/ℓ NaCl, 1.96 g/ℓ $CuSO_4{\cdot}5H_2O$) has permittivity and conductivity equal to those in the simulation. The annular gap between the array and the phantom is filled with HDC pads made using $BaTiO_3$ suspension in deionized water with a volume ratio of 3/7 (V_{BaTiO3}/V_{water}), achieving a permittivity of 150 [9]. A Keysight 85070E Dielectric Probe was used to measure the permittivity of the suspension. The suspension was subsequently packaged in ~5-cm-wide heat-sealable bags (layered polyethylene and polyamide film) to prevent spills and to facilitate arrangement around the phantom.

Coupling between adjacent elements is adjusted using trimmer capacitors located as shown in Figure 4 (b). The capacitor values after trimming are shown in Table II.

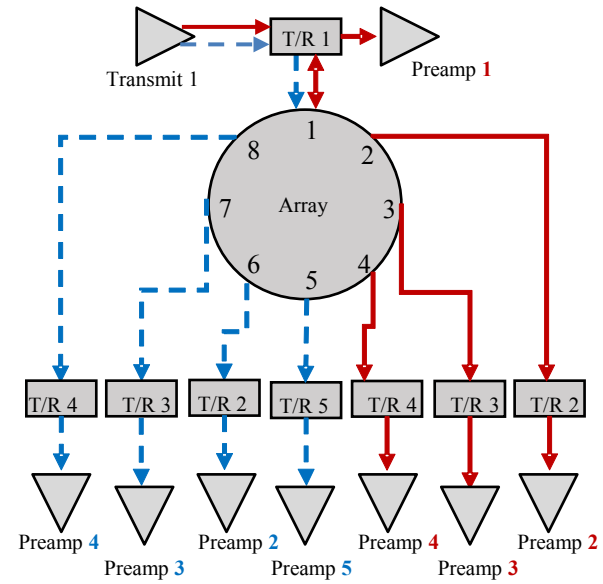

Figure 5: Coil array set-up for imaging (solid line and dashed line connections represent the set-up used for each subset of measurements).

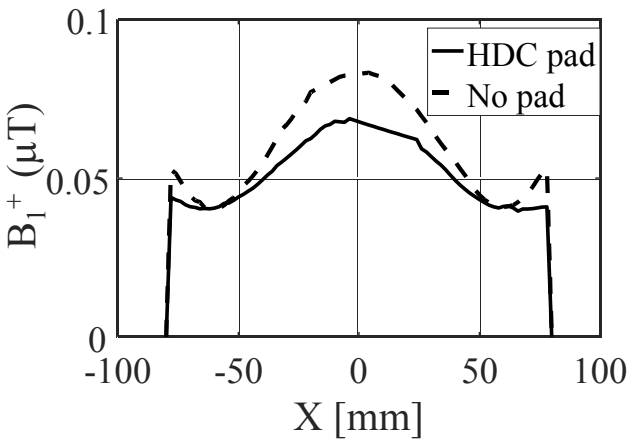

Figure 6: $\mathbf{B}_1^+$ field versus radius plotted in transverse plane in the phantom for coupled coil in presence and without HDC liner.

TABLE II
CAPACITOR VALUES AND LOCATIONS USED FOR FABRICATION.

	C_{t1} (pF)	C_{t2} (pF)	C_d (pF)	d (mm)
Coupled	15	10	-	-
Z_{12}**=0**	15	15	1–15 trimmer	80

D. Measurement

Scattering parameters of the array are measured in the vicinity of 200 MHz using an Agilent 4395A VNA in the presence of dielectric liner and phantom. The structure is supported by foam holders and cables are grounded using a common bulkhead plate. To verify the simulations, the $\mathbf{B}_1^+$ field is measured in the coupled and fully decoupled configurations

using the double-angle method [27] where two gradient-echo images are acquired with nominal flip angles (FA) of 45° and 90°, and the resulting FA map is obtained from the ratio of the image magnitudes. The acquisition parameters are T_E=7 ms, T_R=1000 ms, 192 × 192 × 180 mm^3 FOV, and 1 × 1 × 8 mm^3 resolution.

All images were obtained in a 4.7 T whole-body MRI system using a Unity Inova console (Varian, Palo Alto, California). Because of the availability of a single transmit channel and four receivers in the current scanner, each scan required two acquisitions transmitting with one element and receiving with four channels at a time. The connections for each setup are shown in Figure 5 in dashed and solid lines, respectively.

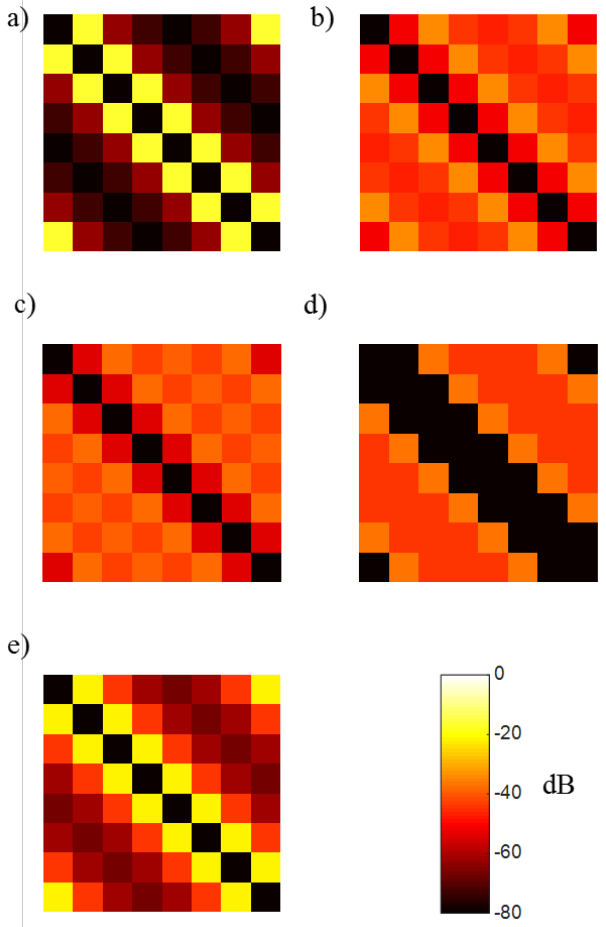

Figure 7: S matrix magnitude (dB) with liner present for (a) coupled, (b) R_{12}=0, (c) X_{12}=0, (d) Z_{12}=0, and (e) coupled without liner.

III. Results and Discussion

A. Simulations

The $\mathbf{B}_1^+$ field is plotted along the diameter of the phantom on a central transverse plane in Figure 6, showing that the liner suppresses the difference between fields at the center versus the peripheral regions of the phantom.

However the drawback of using the HDC liner is the increase in mutual impedance, especially between non-adjacent elements. Figure 7 shows the full scattering matrices for the unlined array as well as for each decoupling case of the lined array, all normalized by matching so that elements on the diagonals are zeros. Removing both terms of the mutual impedance achieves isolation that is better than that obtained when mutual resistance or reactance are removed individually.

TABLE III
Summary of Simulation Results.

	with HDC liner			
	Coupled	R_{12}=0	X_{12}=0	Z_{12}=0
Nearest Neighbor Coupling (dB)	-9.4	-24	-27	-32
Max non-neighbor coupling (dB)	-19	-14	-18	-18
Averaged B_1^+ (nT)	34	34	34.9	39.8
Center B_1^+ (nT)	68.3	64.8	66.5	70.4
Maximum SAR (mW/Kg)	7.3	11	11.9	13.1
Average SAR (mW/Kg)	1.9	2.8	3	3
Deposited power (mW)	7	10.2	10.7	10.8
B_1^+(Avg.)/$\sqrt{Pv}$ ($\frac{\mu T}{\sqrt{W}}$)	0.406	0.336	0.337	0.383
B_1^+(Avg.)/ $\sqrt{SAR(Max)}$ ($\frac{\mu T}{\sqrt{\frac{W}{kg}}}$)	0.398	0.324	0.320	0.347

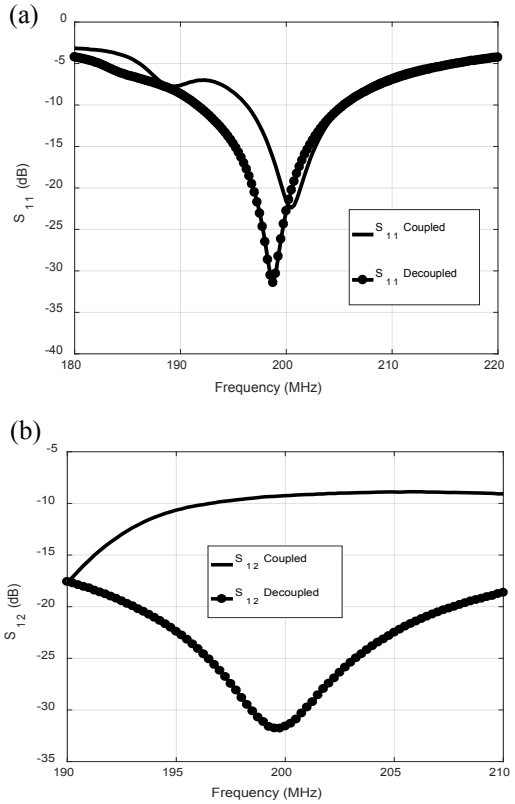

Figure 8: Measured (a) $|S_{11}|$ and (b) $|S_{12}|$ (in dB) between adjacent elements for coupled and decoupled case with the HDC liner.

Removing both terms of mutual impedance reduces nearest-neighbor coupling to -32 dB and other terms to -18 dB or better, thus meeting the requirements set forth in the Introduction (30 and 15 dB, respectively). Conversely, the unlined, coupled coil presents isolations of 28 and 7 dB, respectively. The decoupling achieved in the other cases is shown in Table III. Specifically, if only one term of the mutual impedance is removed, nearest-neighbor isolation is insufficient (27 dB). With the array excited in quadrature the average $\mathbf{B}_1^+$ field magnitude (along with the $\mathbf{B}_1^+$ field at the center of the phantom) is highest with full decoupling. The maximum SAR and

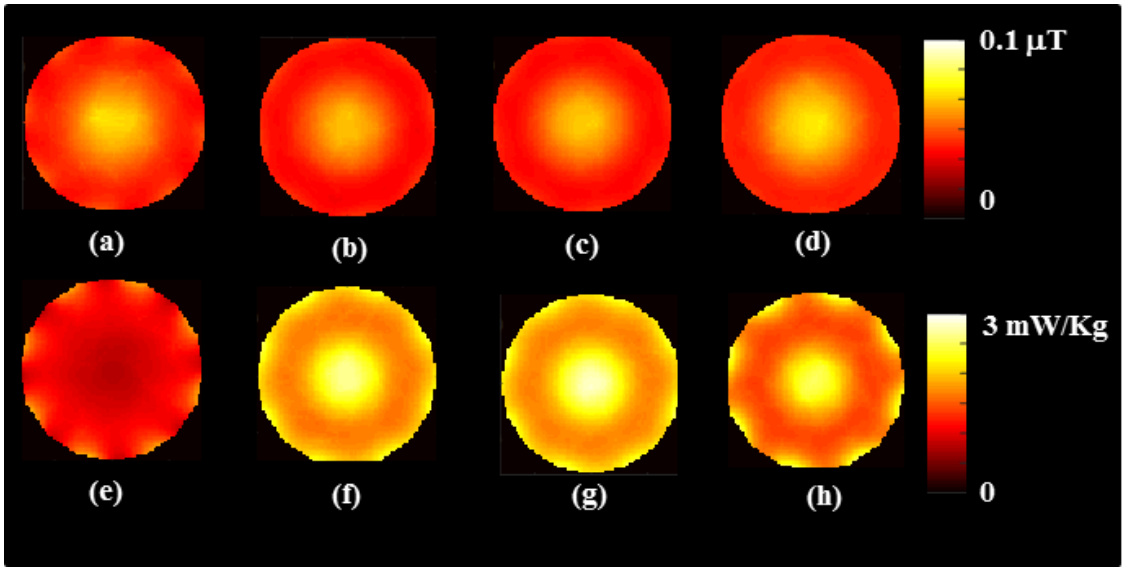

Figure 9: $\mathbf{B}_1^+$ field pattern for (a) coupled, (b) R_{12}=0, (c) X_{12}=0, (d) Z_{12}=0 and corresponding SAR field pattern for (e–h). Each channel is excited with a 1A current source with phase appropriate for circular polarization.

average SAR also increase due to the currents in the additional loops created by the insertion of capacitors between the main loops.

Table III also compares transmit performance in terms of excitation efficiency ($Ev = |\mathbf{B}_1^+|/\sqrt{P_v}$) and safety efficiency ($Sv = |\mathbf{B}_1^+|/\sqrt{\max(SAR_{10g})}$), where P_v is the power deposited in the phantom and max(SAR_{10g}) is the maximum of the 10g SAR average [28]. We observe that decoupling has a minimal influence on the transmit efficiencies, with a small reduction in safety efficiency under full decoupling due to increased maximum SAR.

Using simulation data for electric and magnetic fields, $\mathbf{B}_1^+$ field and SAR patterns are plotted in a transverse slice through the center of the phantom (Figure 9). While the magnetic field patterns remain very similar, SAR increases especially in the peripheral regions of the phantom as a result of currents through the decoupling capacitors.

B. Measurements

Scattering parameters measured on the bench are plotted in Figure 8. Full decoupling eliminates resonant frequency splitting in the $|S_{11}|$ curve and reduces isolation to 32 dB (Figure 8(b)), compared to 9 dB for the coupled case.

The simulated $\mathbf{B}_1^+$field and SAR patterns obtained when only one channel is excited with 1 W of power are plotted in Figure 10 (a)-(d), showing that full decoupling reduces the amount of shared field between two neighboring elements. Moreover, acquired flip angle (= scaled $\mathbf{B}_1^+$) maps are compared to those of the simulation in Figure 10 (e) and (f), confirming better distinction in the transmit field patterns and suppression of signal from neighboring elements.

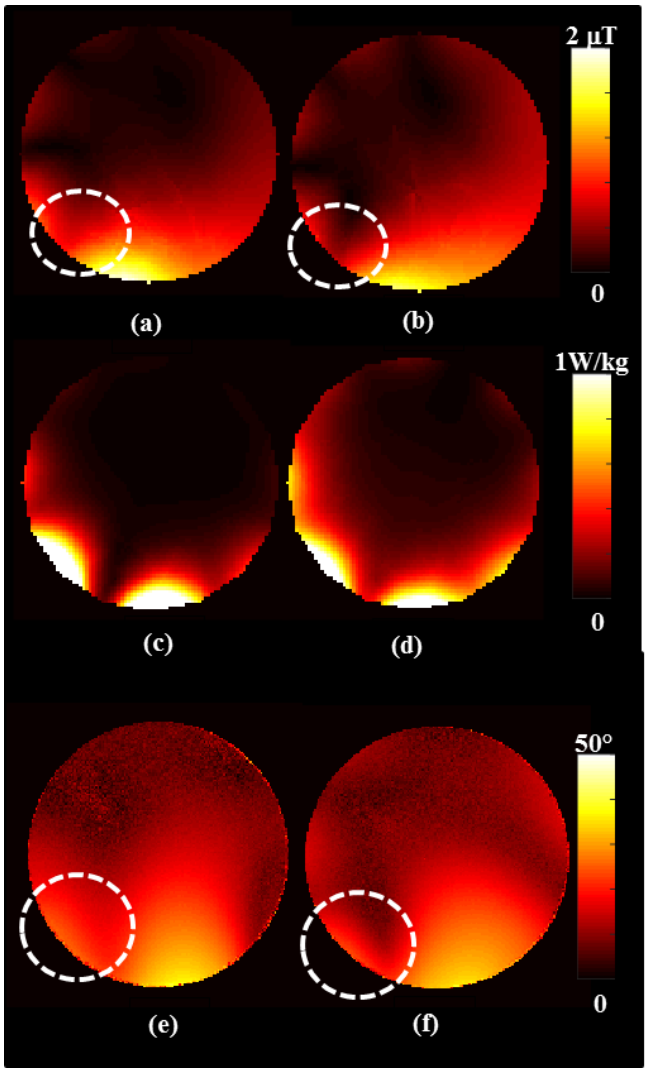

Figure 10: Simulated $\mathbf{B}_1^+$ field (0-2μT) for (a) coupled, (b) decoupled and SAR (0-1W/kg) for (c) coupled and (d) decoupled coil when one channel is excited, flip angle (0-50º) or $\mathbf{B}_1^+$ maps for (e) coupled, (f) decoupled coil.

IV. Conclusion

In this work we investigate the effects of high-permittivity liners and various levels of decoupling on the transmit characteristics of an eight-channel array for imaging the extremities or pediatric brain at 4.7 T. The liner improves field homogeneity but also increases mutual impedance between

elements. This coupling can be reduced to acceptable levels without degrading the transmit performance or field uniformity of the array by removing both resistive and reactive terms of the mutual impedance using capacitive bridges. For each element a distinct field map can therefore be produced as required for parallel transmit techniques (e.g., Transmit SENSE). These methods of array design can be extended readily to larger dimensions or greater numbers of elements.

V. Acknowledgements

The authors thank Messrs. Karim Damji and Peter Šereš for assistance with the MRI measurements and the Canadian Microelectronics Corporation for software access.

VI. References

[1] L. J. B. Pierre-Marie Robitaille, *Ultra high field magnetic resonance imaging*. NY, USA: Springer Science, 2007.

[2] Q. X. Yang, J. Wang, J. Wang, C. M. Collins, C. Wang, and M. B. Smith, "Reducing SAR and enhancing cerebral signal-to-noise ratio with high permittivity padding at 3 T.," *Magn. Reson. Med.*, vol. 65, no. 2, pp. 358–62, Feb. 2011.

[3] A. G. Webb, "Dielectric materials in magnetic resonance," *Concepts in Magnetic Reson. Part A*, vol. 38A, no. 4, pp. 148–184, 2011.

[4] W. Luo, M. T. Lanagan, C. T. Sica, Y. Ryu, S. Oh, M. Ketterman, Q. X. Yang, and C. M. Collins, "Permittivity and performance of dielectric pads with sintered ceramic beads in MRI: early experiments and simulations at 3 T.," *Magn. Reson. Med.*, vol. 70, no. 1, pp. 269–75, Jul. 2013.

[5] W. M. Brink and A. G. Webb, "High permittivity pads reduce specific absorption rate, improve B1 homogeneity, and increase contrast-to-noise ratio for functional cardiac MRI at 3 T," *Magn. Reson. Med.*, vol. 71, no. 4, pp. 1632–1640, 2014.

[6] N. I. Avdievich, J. W. Pan, and H. P. Hetherington, "Resonant inductive decoupling (RID) for transceiver arrays to compensate for both reactive and resistive components of the mutual impedance," *NMR Biomed.*, vol. 26, no. 11, pp. 1547–1554, Nov. 2013.

[7] C. E. Hayes and P. B. Roemer, "Noise correlations in data simultaneously acquired from multiple surface coil arrays," *Magn. Reson. Med.*, vol. 16, no. 2, pp. 181–191, 1990.

[8] P. B. Roemer, W. A. Edelstein, C. E. Hayes, S. P. Souza, and O. M. Mueller, "The NMR phased array," *Magn. Reson. Med.*, vol. 16, no. 2, pp. 192–225, Nov. 1990.

[9] A. Kordzadeh and N. De Zanche, "Optimal permittivity of dielectric liners and their effects on transmit array performance purpose," in *Proc. Intl. Soc. Mag. Reson. Med. 23*, 2015, vol. 38, no. 2, p. 4677.

[10] U. Katscher, P. Bornert, C. Leussler, and J. S. van den Brink, "Transmit SENSE," *Magn. Reson. Med.*, vol. 49, no. 1, pp. 144–150, 2003.

[11] M. Kozlov and R. Turner, "Assessment of decoupling between MRI array elements at 300 MHz," *Prog. Electromagn. Res. Symp. Proc.*, pp. 1020–1024, 2013.

[12] R. F. Lee, R. O. Giaquinto, and C. J. Hardy, "Coupling and decoupling theory and its application to the MRI phased array.," *Magn. Reson. Med.*, vol. 48, no. 1, pp. 203–13, Jul. 2002.

[13] A. M. Maunder, M. Daneshmand, P. Mousavi, B. G. Fallone, and N. De Zanche, "Stray capacitance between magnetic resonance imaging coil elements: models and application to array decoupling," *IEEE Trans. Microw. Theory Techn.*, vol. 61, no. 12, pp. 4667–4677, Dec. 2013.

[14] X. Zhang and A. Webb, "Design of a capacitively decoupled transmit/receive NMR phased array for high field microscopy at 14.1T," *J. Magn. Reson.*, vol. 170, no. 1, pp. 149–55, Sep. 2004.

[15] C. Von Morze, J. Tropp, S. Banerjee, D. Xu, K. Karpodinis, L. Carvajal, C. P. Hess, P. Mukherjee, S. Majumdar, and D. B. Vigneron, "An eight-channel, nonoverlapping phased array coil with capacitive decoupling for parallel MRI at 3 T," *Concepts Magn. Reson. Part B Magn. Reson. Eng.*, vol. 31, no. 1, pp. 37–43, 2007.

[16] J. Jevtic, "Ladder networks for capacitive decoupling in phased-array coils," *Proc. 9th Annu. Meet. ISMRM,* vol. 9, p. 10437, 2001.

[17] M. Weiger, K. P. Pruessmann, C. Leussler, P. Röschmann, and P. Boesiger, "Specific coil design for SENSE: a six-element cardiac array," *Magn. Reson. Med.*, vol. 45, no. 3, pp. 495–504, Mar. 2001.

[18] D. I. Hoult, D. Foreman, G. Kolansky, and D. Kripiakevich, "Overcoming high-field RF problems with non-magnetic Cartesian feedback transceivers.," *MAGMA*, vol. 21, no. 1–2, pp. 15–29, 2008.

[19] I. R. O. Connell, K. M. Gilbert, M. A. Abou-Khousa, and R. S. Menon, "Design of a parallel transmit head coil at 7T with magnetic wall distributed filters," *IEEE Trans. Med. Imaging*, vol. 34, no. 4, pp. 836–845, 2015.

[20] I. R. O. Connell, K. M. Gilbert, M. A. Abou-Khousa, and R. S. Menon, "MRI RF array decoupling method with magnetic wall distributed filters," *IEEE Trans. Med. Imaging*, vol. 34, no. 4, pp. 825–835, 2015.

[21] B. Wu, P. Qu, C. Wang, J. Yuan, and G. X. Shen, "Interconnecting L/C components for decoupling and its application to low-field open MRI array," *Concepts Magn. Reson. Part B Magn. Reson. Eng.*, vol. 31, no. 2, pp. 116–126, Apr. 2007.

[22] C. D. Constantinides, E. Atalar, and E. R. McVeigh, "Signal-to-noise measurements in magnitude images from NMR phased arrays," *Magn. Reson. Med.*, vol. 38, no. 5, pp. 852–857, 1997.

[23] M. Kozlov and R. Turner, "Influence of a dielectric insert of high permittivity on the transmit performance of a 300 MHz multi-channel MRI loop array," *PIERS online*, pp. 116–120, 2011.

[24] A. Kordzadeh and N. De Zanche, "Full mutual coupling suppression in NMR transmit arrays in the presence of high-permittivity pads," in *IEEE International Microwave Symposium (IMS2016)*, 2016, no. 1, pp. 10–13.

[25] R. F. Harrington, *Time-harmonic electromagnetic fields*. IEEE Press : Wiley-Interscience, 2001.

[26] S. M. Wright and L. L. Wald, "Theory and application of array coils in MR spectroscopy.," *NMR Biomed.*, vol. 10, no. 8, pp. 394–410, Dec. 1997.

[27] R. Stollberger and P. Wach, "Imaging of the active B1 field in vivo," *Magn. Reson. Med.*, vol. 38, no. 2, p. 336, 1997.

[28] M. Kozlov and R. Turner, "Influence of shield distance on RF transmit performance for a 7T multi-channel MRI loop array," *Prog. Electromagn. Res. Symp. Proc.*, pp. 255–259, 2012.

Atefeh Kordzadeh received the M.Sc. degree in Electrical Engineering from Iran University of Science and Technology, Tehran. She is currently pursuing her Ph.D. degree with the departments of Biomedical Engineering and Electrical and Computer Engineering at the University of Alberta. Her thesis involves designing radio frequency coils for magnetic resonance imaging, specifically at 4.7 T.

Nicola De Zanche (S'97 – M'03 – SM'15) received the Laurea degree in electronics engineering from the University of Padova, Padova, Italy in 1996 and the Ph.D. degree in medical sciences – biomedical engineering from the University of Alberta, Edmonton, Canada in 2002. He then was a post-doctoral fellow and subsequently senior scientist at the Institute for Biomedical Engineering of the Swiss Federal Institute of Technology (ETH Zurich) and the University of Zurich. In 2008 he joined the Division of Medical Physics, Department of Oncology of the University of Alberta where is now Associate Professor. His research interests include all aspects of RF technology for MRI.